Catalysis Science & Technology

PAPER

Synthesis and characterization of fibrous silica ZSM-5 for cumene hydrocracking†

M. L. Firmansyah,[a] A. A. Jalil,*[bc] S. Triwahyono,[ad] H. Hamdan,[e] M. M. Salleh,[d] W. F. W. Ahmad[d] and G. T. M. Kadja[f]

Cite this: *Catal. Sci. Technol.*, 2016, **6**, 5178

Received 15th January 2016,
Accepted 11th March 2016

DOI: 10.1039/c6cy00106h

www.rsc.org/catalysis

Inspired by the high accessibility and low diffusion limitations of fibrous silica nanoparticles (KCC-1), fibrous silica ZSM-5 (FZSM-5) was engineered using a microemulsion system. The spherical FZSM-5 with a dendrimeric silica fiber possessed a high surface area (554 m^2), a wide pore diameter (2–20 nm), abundant strong acid sites and high catalytic activity towards cumene hydrocracking.

Zeolites are aluminosilicate minerals with interconnected channels with various shapes, structures, topologies, and compositions, which have diverse properties and industrial applications. ZSM-5 is one of the most commonly used zeolites in industry due to its high thermal stability, shape selectivity and a wide range of tunable acidities and crystal sizes. However, the microporous structure of ZSM-5 imposes drawbacks such as low active site accessibility and diffusion limitations, which may lead to rapid catalyst deactivation. Therefore, the development of mesoporous ZSM-5 that possesses both micropore and mesopore structures may improve the catalytic activity and stability as it increases the reactant diffusion capability into the ZSM-5 pores. A common method to obtain mesoporous ZSM-5 is the post-synthetic demetallation (desilication or dealumination)[1] method. However, post-synthetic demetallation can partially destroy the structure, leading to the loss of acidic sites. The soft templating method is another approach to obtain mesopore structures in zeolites. The flexible supramolecular templates allow for controlling and generating both micropore and mesopore structures. Recently, soft templating using a surfactant produced a new morphology of a mesoporous silica material having dendrimeric silica fibers.[2] Silica nanoparticles, which possess dendrimeric silica fiber morphology (KCC-1), have been explored as support materials in catalysis and adsorption processes. Dendrimeric silica fibers that widen radially outward provide a high surface area and can enhance the accessibility of the functional materials to the reactant.[3–5] KCC-1 also possess intrinsic mesopores and exhibit high thermal stability and activity.[2] Preparation of these materials utilizes a microemulsion system containing a surfactant, oil and water.

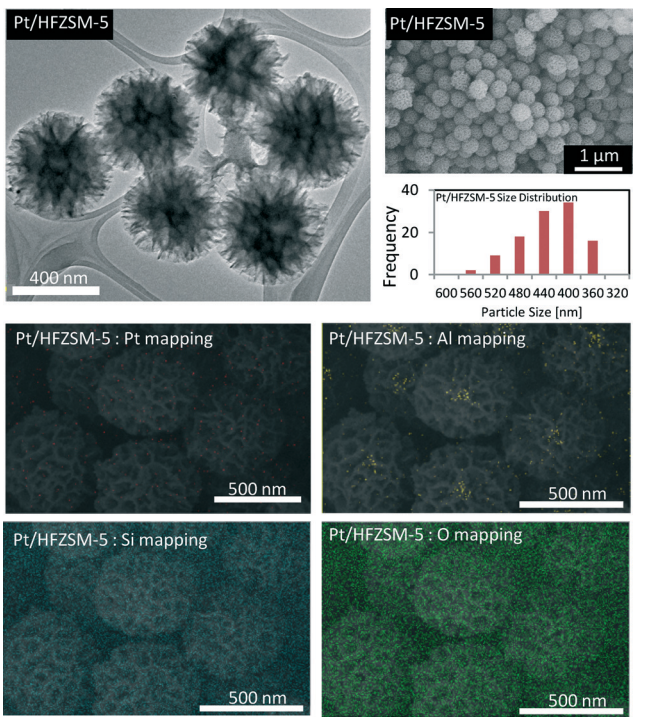

Fig. 1 TEM, FESEM, particle size distribution and elemental mapping of Pt/HFZSM-5.

[a] *Department of Chemistry, Faculty of Science, Universiti Teknologi Malaysia, 81310 UTM Johor Bahru, Johor, Malaysia*
[b] *Center of Hydrogen Economy, Institute of Future Energy, Universiti Teknologi Malaysia, 81310 UTM Johor Bahru, Johor, Malaysia. E-mail: aishahaj@utm.my*
[c] *Department of Chemical Engineering, Faculty of Chemical and Energy Engineering, Universiti Teknologi Malaysia, 81310 UTM Johor Bahru, Johor, Malaysia*
[d] *Centre for Sustainable Nanomaterials, Ibnu Sina Institute for Scientific and Industrial Research, Faculty of Science, Universiti Teknologi Malaysia, 81310 UTM Johor Bahru, Johor, Malaysia*
[e] *UTM Razak School of Engineering and Advanced Technology, Universiti Teknologi Malaysia, 54100 UTM Kuala Lumpur, Malaysia*
[f] *Department of Inorganic and Physical Chemistry, Faculty of Mathematics and Natural Sciences, Institut Teknologi Bandung, Jl Ganesha 10, Bandung 40132, Indonesia*

† Electronic supplementary information (ESI) available. See DOI: 10.1039/c6cy00106h

Furthermore, KCC-1 allow for facile control over the particle size and morphology by the introduction of a co-surfactant and various co-solvents.[6,7] Fihri *et al.*[4] reported that Ru/KCC-1 exhibited better catalytic performance in hydrogenolysis compared with Ru/SBA-15 and Ru/MCM-41, due to better accessibility to the active sites. In this present work, we reported a novel fibrous morphology of ZSM-5, which was prepared by using a microemulsion system coupled with zeolite crystal-seed crystallization.

Fibrous silica ZSM-5 (FZSM-5) was prepared by using a microemulsion technique coupled with zeolite seed-assisted crystallization. The microemulsion formed from the combination of a surfactant (CTAB), an oil phase (toluene), water, and a co-surfactant (butanol). The mixture was treated under hydrothermal conditions for 4 h. The calcined solid product was then exposed to protonation and impregnation with platinum (details are given in the ESI†).

The morphology and particle size distribution of platinum loaded on protonated fibrous silica ZSM-5 (Pt/HFZSM-5) are shown in Fig. 1. Pt/HFZSM-5 possessed a spherical and narrow particle size distribution (360–560 nm) with a well-ordered dendrimeric morphology. Elemental mapping showed widely distributed Si atoms, and that Al atoms were mainly distributed on the center of each sphere. Pt atoms were scarcely distributed on the Pt/HFZSM-5 particles. It was noted that Pt/HFZSM-5 showed a completely different morphology from that of Pt/HZSM-5 (Fig. S1†). The aluminosilicate framework of ZSM-5 was mainly distributed on the center of the Pt/HFZSM-5 sphere and the dendrimer was mainly composed of silica and a small part of the ZSM-5 framework. It also exhibited a distance between dendrimers (inter-dendrimer distance) which would allow for easy diffusion of reactants, leading to increased catalytic performance.

The FZSM-5 type catalyst showed the characteristic pattern of an MFI structure at 2θ = 7–10° and 20–24° (Fig. 2A).[8] No significant changes were observed after the protonation and introduction of Pt. Moreover, there was an absence of diffraction peaks of Pt in Pt/HFZSM-5 and Pt/HZSM-5.[9] This was probably due to the poor crystallinity of the platinum species or an amount of Pt that is below the detection limit of the instrument. Furthermore, in general, the FZSM-5 type catalyst possessed lower crystallinity than the ZSM-5 type catalyst due to the formation of dendrimeric silica fibers on ZSM-5 (Table S1†). The FZSM-5 type catalyst also showed a significant increase in the Si/Al ratio than the ZSM-5 type catalyst (Table S1†). This was attributed to the presence of the dendrimeric silica fiber and the decrease in the alumina species of the FZSM-5 type catalyst. Here, we propose that formation of a core–shell FZSM-5 occurred with ZSM-5 as the core and the dendrimeric silica fibers as the shell, which is supported by the TEM, FESEM, elemental mapping, and XRD results.

According to the ^{27}Al MAS NMR spectra in Fig. 2B, HFZSM-5 showed a chemical shift at 60 ppm while HZSM-5 exhibited a shift at 55 ppm, which could be associated with an increasing amount of isolated tetrahedrally coordinated aluminum atoms[10] in HFZSM-5. However, the decrease in signal intensity between 50–60 ppm could be attributed to the removal of tetrahedrally coordinated framework Al atoms for extraframework Al atoms, which is supported by the higher signal intensity at 0 ppm of HFZSM-5 than that of HZSM-5. The ^{29}Si MAS NMR spectra of both catalysts showed a dominant signal at −114 ppm which was assigned to the crystallographically equivalent site of $(\equiv SiO)_4Si$ for both HFZSM-5 and HZSM-5 (ref. 11) (Fig. S2†). HFZSM-5 shows a higher signal intensity than HZSM-5 due to an additional silicate framework from the formation of dendrimeric silica fibers. In accordance with the XRD patterns, the tetrahedral alumina and silica species of FZSM-5 were presented in the ZSM-5 framework.

The FZSM-5 and ZSM-5 type catalysts exhibited four absorbance peaks in the OH stretching region. The absorbance bands at 3740, 3660 and 3610 cm^{-1} were observed for both the FZSM-5 and ZSM-5 type catalysts, which were assigned to the stretching vibrations of the silanol groups on the external surface, hydroxyl groups bonded to the extraframework alumina, and bridging hydroxyl groups, respectively.[12,13] Additionally, the stretching vibrations of perturbed hydroxyl groups by lattice defects at 3700 cm^{-1} was only observed for the FZSM-5 type catalyst (Fig. S3A†).[12] This was probably due to the presence of dendrimeric silica fibers in FZSM-5. The FZSM-5 type catalyst exhibited a higher intensity of the band at 3740 cm^{-1} than the ZSM-5 type catalyst, which could be attributed to the additional terminal silanol groups from the formation of the dendrimeric silica fibers. In agreement with the NMR results, the FZSM-5 type catalyst possessed more extraframework alumina species than the ZSM-5 type catalyst. The FZSM-5 type catalyst also exhibited absorbance bands at 2000, 1890 and 1630 cm^{-1}, which were ascribed to the vibrational overtones and combination framework modes of the T–O units of the zeolite framework (Fig. S3B†).[12] No apparent changes in lattice stretching after protonation and impregnation could indicate the stability of the aluminosilicate framework in FZSM-5. Based on the elemental mapping, XRD, NMR and IR results, FZSM-5 possessed the ZSM-5 framework

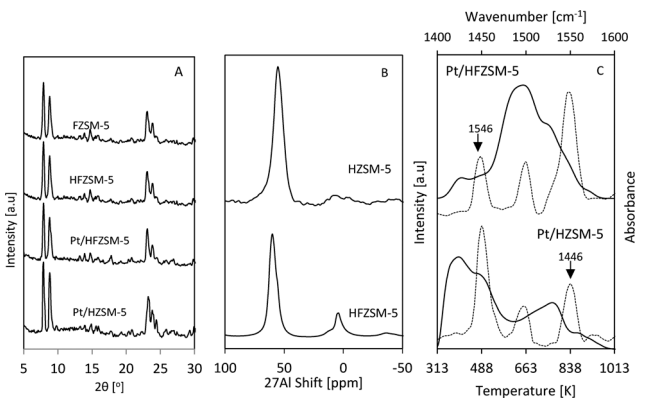

Fig. 2 (A) XRD patterns of all the catalysts, (B) ^{27}Al NMR spectra, and (C) NH_3-TPD profile (true line) and pyridine IR spectra (dotted line) after outgassing at 623 k.

structure, which was concentrated on the center of each dendritic sphere.

According to the N_2 adsorption–desorption isotherms of the catalysts, the ZSM-5 type catalyst exhibited typical isotherms for microporous materials. Meanwhile, the FZSM-5 type catalyst showed typical type IV isotherms with H_3 hysteresis, showing a mesoporous material with non-uniform slit-shaped pores (Fig. S4A†).[7] Higher nitrogen uptake was demonstrated by the FZSM-5 type compared to the ZSM-5 type catalyst, indicating the higher porosity of the FZSM-5 type catalyst. For all the catalysts, nitrogen uptake at a low relative pressure was due to the presence of micropores. At high relative pressures, a sharp increase in nitrogen uptake due to the presence of interparticle pores was observed only in the FZSM-5 type catalyst. The pore distributions derived from the NLDFT method showed sharp peaks in the range of 2–5 nm and small peaks in the range of 10–20 nm, corresponding to the mesopores from the self-assembly of the CTAB surfactant and the inter-dendrimer distances, respectively (Fig. S4B†). The presence of dendrimers may be responsible for the significant increase in the BET surface area and pore volume of the FZSM-5 type catalyst. The inter-dendrimer distances of FZSM-5 could be counted as mesopores and caused a significant difference in the mesopore volume between the FZSM-5 and the ZSM-5 type catalysts. Pt/HFZSM-5 showed an increase of about 95% in the BET surface area compared to that of Pt/HZSM-5. In fact, about 50% of the surface area of Pt/HZSM-5 was dominated by the micropore surface area due to the absence of dendrimeric silica fibers (Table S1†). Besides, it also displayed a relatively small total pore volume and mesopore volume compared to those of the FZSM-5 type catalyst. Upon the introduction of Pt into the protonated fibrous silica ZSM-5 (HFZSM-5), slight decreases in the surface area and total pore volume were observed. This could be attributed to micropore blockage and a reduction in interparticle porosity due to the decrease in the micropore surface area and mesopore volume in Pt/HFZSM-5.

Fig. 2C shows the NH_3-TPD profiles of Pt/HFZSM-5 and Pt/HZSM-5. Pt/HFZSM-5 was dominated by moderate and strong acid sites, as evidenced by the high intensity of the peaks at around 500–830 K. Meanwhile, Pt/HZSM-5 was dominated by relatively weak and moderate acid sites, as indicated by the higher signal intensity at around 313–500 K than the signal intensity at around 600–850 K. The distribution of acid strength was also assessed by using a titration method with a Hammett indicator. Pt/HFZSM-5 exhibited a higher amount of total acid sites compared with Pt/HZSM-5. The significant increase in the acid sites with acid strength $+4.8 \leq H_o \leq +6.8$ could be attributed to the increase in the number of extraframework alumina and the presence of a dendrimeric silica fiber, which increase the number of acid sites of the silanol group.[14] Pt/HFZSM-5 also showed a significant increase in the acid sites with acid strength $H_o \leq +3.3$. This increase in the strong acid sites of Pt/HFZSM-5 could be associated with the increase in the number of isolated Al atoms in the framework.[15] This result was supported by the chemical shift in the ^{27}Al MAS NMR spectra at 60 ppm, which was assigned to the formation of an isolated AlO_4 tetrahedral. On the other hand, the ZSM-5 ^{27}Al MAS NMR spectra showed a chemical shift at 55 ppm.[10]

Using pyridine as a probe, the FTIR spectra obtained after outgassing at 623 K showed that the FZSM-5 and ZSM-5 type catalysts exhibited absorbance bands at 1446 and 1546 cm^{-1}, respectively, as shown in Fig. 2C. These were associated with the presence of both Lewis and Brønsted acid sites for all catalysts.[16] An intense band at 1446 cm^{-1} for the FZSM-5 type catalyst indicated the presence of abundant Lewis acid sites on FZSM-5, which may be due to the presence of Si–OH electron pair acceptors in the dendrimeric silica fibers and the exposed surface of unsaturated cations of the FZSM-5 type catalyst.[17] The introduction of Pt could change the amount of Brønsted acid sites of HFZSM-5 which may correspond to the dehydroxylation process resulting in the increase in the number of Lewis acid sites.[19] The increase in the number of Lewis acid sites could also be attributed to the interaction of the electron-deficient Pt with pyridine.[20] On the contrary, Pt/HZSM-5 exhibited a higher intensity of the band at 1546 cm^{-1}, indicating the presence of a higher number of Brønsted acid sites which arises from bridging hydroxyl groups (SiOHAl). After outgassing with pyridine at 623 K, the FZSM-5 type catalyst exhibited a higher concentration of Lewis acid sites than Brønsted acid sites.[18] Meanwhile, the ZSM-5 type catalyst exhibited a higher concentration of Brønsted acid sites than Lewis acid sites (Table S1†). In accordance with the NH_3-TPD results, the moderate and strong acid sites of Pt/HFZSM-5 were probably dominated by the Lewis acid sites, while for Pt/HZSM-5, the strong acid sites were probably dominated by the Brønsted acid sites.

Cumene hydrocracking was used to assess the catalytic activities of the FZSM-5 type catalysts in the temperature range of 373–623 K. Fig. 3A shows the comparison of cumene hydrocracking activities of FZSM-5, HZSM-5, HFZSM-5, Pt/HFZSM-5, and Pt/HZSM-5. At 623 K, Pt/HFZSM-5 exhibited the highest rate of conversion of 0.303 μmole s^{-1} g_{cat}^{-1},

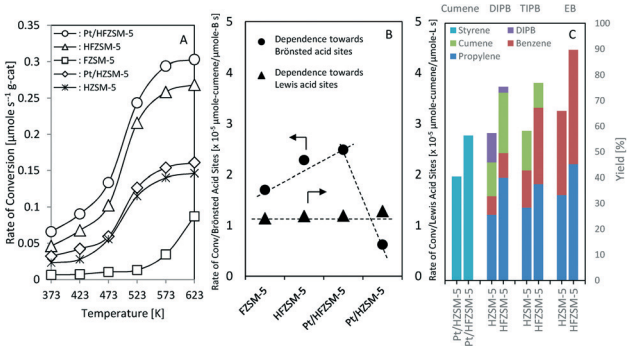

Fig. 3 (A) Rate of cumene conversion as a function of reaction temperature, (B) dependence of the cumene rate of conversion of all the catalysts on Brønsted and Lewis acid sites after outgassing at 623 K, and (C) product yields of cumene, DIPB, and TIPB hydrocracking over HFZSM-5 and HZSM-5 at 573 K and EB dehydrogenation over Pt/HFZSM-5 and Pt/HZSM-5 at 773 K.

followed by HFZSM-5 (0.268 μmole s^{-1} g_{cat}^{-1}), Pt/HZSM-5 (0.161 μmole s^{-1} g_{cat}^{-1}), HZSM-5 (0.146 μmole s^{-1} g_{cat}^{-1}) and FZSM-5 (0.087 μmole s^{-1} g_{cat}^{-1}). The product distribution of cumene hydrocracking was equally composed of propylene and benzene. Pt/HFZSM-5 gave a total product yield of 89.5%, while FZSM-5, HZSM-5, HFZSM-5 and Pt/HZSM-5 gave total product yields of 12.1, 79.8, 69.8 and 65.8% at 573 K, respectively. Pt/HFZSM-5 displayed high catalytic stability which could maintain 88% conversion while the catalytic activity of Pt/HZSM-5 decreased by 15% after 100 doses of cumene (Fig. S5†). This could be attributed to the lower amount of coke deposited on Pt/HFZSM-5 compared with that on Pt/HZSM-5 (Fig. S6†) during the reaction due to the presence of intrinsic mesopores.[21] The formation of the dendrimeric silica fiber increased the total amount and strength of the acid sites which led to the higher catalytic activity of Pt/HFZSM-5 compared to Pt/HZSM-5. Pt/HFZSM-5 showed up to 80% increase in the rate of conversion compared to Pt/HZSM-5. Fig. 3B shows the plot of the dependence of the rate of conversion of all the catalysts on acid site concentration after outgassing at 623 K. There was no significant change in the yield ratio of the rate of conversion to the Lewis acid site concentration, which could be attributed to the clear correlation between the concentration of Lewis acid sites and the rate of cumene hydrocracking.[22] The presence of intrinsic mesopores also allowed for the high diffusion rates of the products and/or reactants, while the inter-dendrimer distances of the FZSM-5 type catalyst promoted facile access to the active sites. These properties enhanced the catalytic activity of the FZSM-5 type catalyst. Thus, cumene (critical diameter = 7.8 Å) would not suffer any diffusional limitations when diffusing through the FZSM-5 type catalyst.[23] On the other hand, the ZSM-5 type catalyst with a microporous structure would impose diffusional limitations, which lead to lower catalytic activity. The introduction of Pt was able to increase the acid sites in HFZSM-5 and provided molecular hydrogen from a hydrogen spillover phenomenon to assist in the formation of protonic acid sites.[24] In general, the activity and stability of the FZSM-5 type catalysts were better than or comparable to other zeolites and/or mesoporous materials[25] in the literature, as illustrated in Table S3.†

In order to evaluate the activity of the FZSM-5 and ZSM-5 catalysts on molecules of different sizes, HFZSM-5 and HZSM-5 were examined for 1,4-diisopropylbenzene (DIPB) and 1,3,5-triisopropylbenzene (TIPB) hydrocracking at 573 K. HFZSM-5 exhibited higher catalytic activity in both DIPB and TIPB hydrocracking than HZSM-5 (Table S2†). Fig. 3C shows the products of DIPB and TIPB hydrocracking. Since DIPB and TIPB possess critical diameters of 8.4 Å and 9.5 Å, respectively, hydrocracking of these molecules with conventional ZSM-5 (pore size = 5.7 Å) might be limited by the diffusion problem.[26] With conventional ZSM-5, DIPB and TIPB cracking occur solely on the external surface of ZSM-5, with fewer active sites due to the diffusion limitation in the micropores.[26,27b] However, the mesopores and inter-dendrimer distances of HFZSM-5 increased the diffusion rates and active site accessibility of large molecules such as DIPB and TIPB, leading to the higher catalytic activity of HFZSM-5 than that of HZSM-5.[26,27]

The production of styrene from ethyl benzene (EB) *via* the dehydrogenation route was performed on Pt/HFZSM-5 and Pt/HZSM-5 in 56.3 and 40.3% styrene yield, respectively. In the dehydrogenation reaction, a high temperature or low pressure is required for the high conversion of EB because of the endothermic reaction. Platinum was used because it is a highly active catalytic element and is not required in large quantities. Pt/HFZMS-5 gave a higher styrene yield compared to other materials (Table S3†). The selectivity and activity during dehydrogenation are strongly influenced by the degree of platinum dispersion.[28a] Pt/HFZSM-5 possessed a high surface area and a large pore diameter, which led to a higher dispersion degree and smaller size of the Pt particle compared to Pt/HZSM-5 (Table S1†). The dendrimeric silica fibers in Pt/HFZSM-5 could also decrease the diffusional resistance of the reactant. These properties could enhance the activity and selectivity of Pt/HFZSM-5, since the activity was strongly influenced by the metal particle dispersion degree and the selectivity was limited by the mass transfer rate.[29] The catalytic activity of commercial ZSM-5 with similar Si/Al ratio to the FZSM-5 type catalyst was also assessed in all catalytic reactions. HZSM-5(50) present much lower catalytic activity compared to the FZSM-5 type catalyst (Table S2†). The presence of a dendrimeric silica fiber on the FZSM-5 type catalyst provides more Lewis acid sites which have direct correlation with the catalytic activity of the catalyst. Moreover, the microporosity of HZSM-5(50) increases the diffusion limitations of the reactants which decreases their catalytic activity.

The formation of fibrous silica ZSM-5 is due to the combination of zeolite crystal-seed crystallization method and microemulsion system as the template. The ZSM-5 seed acted as a nucleation site wherein initial-bred nuclei were formed on the seed surface and then dislodged from the surface. The crystallization process may have occurred in a small portion of the ZSM-5 seed. Desilication and partial dealumination of the ZSM-5 seed may have occurred during the dislodging in some parts of ZSM-5. This phenomenon led to the increase in perturbation of the hydroxyl groups and extraframework alumina species. The formation of a fibrous morphology involved a bicontinuous microemulsion based on CTAB. The ZSM-5 nuclei could bind to the head groups of the cationic surfactant due to the columbic interaction between the negatively charged ZSM-5 framework and the positively charged surfactant hydrophilic groups, as observed in the silicate–surfactant interaction.[7] ZSM-5 was probably surrounded by the surfactant molecules and the microemulsions formed simultaneously. A closed structured micelle was produced from the bicontinous microemulsions due to an increase in water–oil interface between surfactant layers. This process occurred simultaneously with the percolation of the micelle spheres which led to the formation of a dendrimeric template. These micelle aggregates were interconnected by their water layers

and the ZSM-5 nuclei underwent crystallization in these water layers. Eventually, a zeolite with a core–shell structure was formed, where the core parts were grown from ZSM-5 seeds and the dendrimeric silica fibers as the shell parts were grown from hydrolyzed TEOS.

In summary, ZSM-5 with dendrimeric silica fibers was successfully prepared by combining the microemulsion template and the zeolite crystal-seed crystallization methods. FZSM-5 possessed outstanding physicochemical properties, including a high surface area, a dendrimeric surface morphology, and abundant strong acid sites. The excellent activity of FZSM-5 in cumene, DIPB and TIPB hydrocracking, as well as in EB dehydrogenation could be attributed to the high amount and high accessibility of the active sites and also the high dispersion of the metal particle due to the large surface area of the FZSM-5 type catalyst. Protonation and introduction of Pt into the FZSM-5 type catalyst further enhanced the catalytic activity towards cumene hydrocracking and EB dehydrogenation.

Acknowledgements

A part of this work was supported by the Nippon Sheet Glass Foundation for Materials Science and Engineering, Japan (No. 4B181) and the Research University Grant (No. 00M67) of Universiti Teknologi Malaysia, Malaysia.

Notes and references

1 D. Verboekend and J. Perez-Ramirez, *Catal. Sci. Technol.*, 2011, **1**, 879.
2 V. Polshettiwar, D. Cha, X. Zhang and J. M. Basset, *Angew. Chem., Int. Ed.*, 2010, **49**, 9652.
3 V. Polshettiwar, J. Thivolle-Cazat, M. Taoufik, F. Stoffelbach, S. Norsic and J. M. Basset, *Angew. Chem., Int. Ed.*, 2011, **50**, 2747.
4 A. Fihri, M. Bouhrara, U. Patil, D. Cha, Y. Saih and V. Polshettiwar, *ACS Catal.*, 2012, **2**, 1425.
5 R. K. Sharma, S. Sharma, S. Dutta, R. Zboril and M. B. Gawande, *Green Chem.*, 2015, **17**, 3207.
6 D. S. Moon and J. K. Lee, *Langmuir*, 2014, **30**, 15574.
7 D. S. Moon and J. K. Lee, *Langmuir*, 2012, **28**, 12341.
8 K. Shen, N. Wang, W. Qian, Y. Cui and F. Wei, *Catal. Sci. Technol.*, 2014, **4**, 3840.
9 J. Shi, L. Chen, N. Ren, Y. Zhang and Y. Tang, *Chem. Commun.*, 2012, **48**, 8583.
10 J. Dedecek, S. Sklenak, C. Li, F. Gao, J. Brus, Q. Zhu and T. Tatsumi, *J. Phys. Chem. C*, 2009, **113**, 14454.
11 L. P. Teh, S. Triwahyono, A. A. Jalil, C. R. Mamat, S. M. Sidik, N. A. A. Fatah, R. R. Mukti and T. Shishido, *RSC Adv.*, 2015, **5**, 64551.
12 H. D. Setiabudi, A. A. Jalil, S. Triwahyono, N. H. N. Kamarudin and R. R. Mukti, *Appl. Catal., A*, 2012, **417**, 190.
13 K. A. Tarach, J. Tekla, W. Makowski, U. Filek, K. Mlekodaj, V. Girman, M. Choi and K. Gora-Marek, *Catal. Sci. Technol.*, 2016, DOI: 10.1039/C5CY01866H.
14 K. Wang, X. Wang and G. Li, *Microporous Mesoporous Mater.*, 2009, **94**, 325.
15 H. Stach, J. Janchen and U. Lohse, *Catal. Lett.*, 1992, **13**, 389.
16 P. Sreenivasulu, N. Viswanadham, T. Sharma and B. Sreedhar, *Chem. Commun.*, 2014, **50**, 6232.
17 N. Topsøe, K. Pedersen and E. G. Derouane, *J. Catal.*, 1981, **70**, 41.
18 C. A. Emeis, *J. Catal.*, 1993, **141**, 347.
19 L. B. Uytterhoeven, L. G. Cristner and W. K. Hall, *J. Phys. Chem.*, 1965, **69**, 2117.
20 D. Kubička, N. Kumar, T. Venäläinen, H. Karhu, I. Kubičkova, H. Österholm and D. Y. Murzin, *J. Phys. Chem. B*, 2006, **110**, 4937.
21 R. Srivastava, M. Choi and R. Ryoo, *Chem. Commun.*, 2006, 448.
22 A. H. Karim, S. Triwahyono, A. A. Jalil and H. Hattori, *Appl. Catal., A*, 2012, **433**, 49.
23 S. Al-Khattaf and H. de Lasa, *Appl. Catal., A*, 2002, **226**, 139.
24 (*a*) T. Shishido and H. Hattori, *Appl. Catal., A*, 1996, **146**, 157; (*b*) N. H. R. Annuar, A. A. Jalil, S. Triwahyono and Z. Ramli, *J. Mol. Catal. A: Chem.*, 2013, **377**, 172.
25 (*a*) Z. Xue, J. Ma, J. Zheng, T. Zhang, Y. Kang and R. Li, *Acta Mater.*, 2012, **60**, 5712; (*b*) Y. Nie, S. Shang, X. Xu, W. Hua, Y. Yue and Z. Gao, *Appl. Catal., A*, 2012, **433**, 69.
26 K. A. Mahgoub and S. Al-Khattaf, *Energy Fuels*, 2005, **19**, 329.
27 (*a*) C. Yin, L. Feng, R. NI, L. Hu, X. Zhao and D. Tian, *Powder Technol.*, 2014, **253**, 10; (*b*) X. H. Vu, U. Bentrup, M. Hunger, R. Kraehnert, U. Armbuster and A. Martin, *J. Mater. Sci.*, 2014, **49**, 5676.
28 (*a*) C. Moran, E. Gonzalez, J. Sanchez, R. Solano, G. Carruyo and A. Moronta, *J. Colloid Interface Sci.*, 2007, **315**, 164; (*b*) A. Sun, Z. Qin and J. Wang, *Appl. Catal., A*, 2002, **234**, 179.
29 B. V. Vora, *Top. Catal.*, 2012, **55**, 1297.

